Progress In Electromagnetics Research M, Vol. 103, 141–149, 2021

Polarization Sensitive Dual-Band Metasurface Lens for X-Band Applications

Pallapati Vinod Kumar* **and Basudeb Ghosh**

Abstract—This paper presents a dual-band polarization dependent phase gradient metasurface (PGMS) lens based on phase compensation method. The proposed metasurface (MTS) consists of a multi-layered unitcell with elliptical structures encircled by a square loop. Owing to the elliptical shape, the unitcell produces an independent phase control for different polarizations of incident wave at two operating frequencies. The present work is aimed to design a dual-band gain enhancement MTS lens antenna in the broadside direction at 10 GHz and 12 GHz. The proposed MTS is designed by one-to-one spatial phase mapping with major and minor axes of the elliptical unitcell at 10 and 12 GHz for x- and y-polarized incident waves, respectively. The performance of the MTS is validated by placing two linearly polarized patch antennas operating at 10 GHz and 12 GHz at the focal distance. The simulation and measured results show a gain enhancement of 10 dB in the frequency range of [9.5–10.1] GHz and [11.6–12.1] GHz for x- and y-polarized waves, respectively.

1. INTRODUCTION

Deep space vehicles and advanced cube satellites for space applications open a new area of research in antenna systems with low power consumption [1]. Traditional CubeSat consists of phased arrays [2] and inflatable antennas [3] operating at X-band in LEO orbits. However, in deep space missions, the antenna should have larger gain due to the limited RF power. Recently, JPL has carried out an extensive work on MTS antennas in developing medium to high gain antennas for CubeSat, i.e., MarCO [2], ISARA [4], and OMERA [5]. MTS antennas have the advantage of simple and low cost with low side lobe level. MTS characteristics are defined by the engineered structure called unitcell and its spatial arrangement. A majority of the MTS based devices and antennas operate on the principle of resonating and non-resonating characteristics of the unitcell [6–9]. The resonance characteristics of unitcells have been widely used for sensing [10] and stealth applications [11]. However, non-resonating characteristics have found applications in beam controlling [12–17] and RCS reduction [18]. The non-resonance characteristics on the MTS with gradient phase profiles result in PGMS [13, 19]. The PGMSs with linear [9] and nonlinear [17, 20] phase variations are proposed to control the reflected or transmitted wave characteristics. Another major application of PGMS is to collimate the beam in a given direction to realize high gain antennas [15, 21]. Several PGMS based high gain antennas are proposed in [14, 17, 20, 22].

However, much of the available literature concentrates on the design of PGMS antenna for reflecting and transmitting arrays for a single frequency operation. Multi-band MTS has attracted an enormous attention from the scientific community for improving the communication quality and integrating several applications into a single device, thereby, reducing the cost. Multi-band resonator [22, 23] and multi-mode MTS [24–29] are proposed to realize multi-band MTS characteristics. However, the design of a multi-band PGMS based high gain antenna poses a huge challenge. Maintaining a controllable

Received 16 May 2021, Accepted 24 June 2021, Scheduled 16 July 2021
* Corresponding author: Pallapati Vinod Kumar (vinodkumar.iist@gmail.coms).
The authors are with the Indian Institute of Space Science and Technology, India.

and independent phase at different frequencies is a challenging task due to strong coupling between the elements. A very limited literature dealing with dual-band high gain PGMS antennas has been reported [22, 30–32].

A dual and triple band circularly polarized reflect array is presented in [22] by designing a super cell consisting of different unitcells operating at multiple bands. However, for linearly polarized (LP) MTS lens, it is difficult to realize a super cell containing multiple elements operating in different bands due to the strong coupling between the unitcell elements. Alternatively, the LP-transmitted wave can be controlled by the polarization of the incident wave [26]. Using the polarization dependency, dual-band lenses in X/Ku band [30, 31] and C/X band [32] have been designed and analyzed. The present paper aims to design a dual-band high gain PGMS antenna at X-band. Most of the earlier literature deals with the rectangular patches or cross-slots to achieve dual band operations. This paper presents a complete study on a novel elliptical unitcell in order to improve the lens performance in terms of the gain enhancement and side lobe level (SLL) reduction. Circular patch MTS has been proposed to achieve high gain at a single frequency [17]; however, to the best of authors knowledge, the realization of polarization-sensitive dual-band gain enhancement using an elliptical unitcell is not reported in the literature. The idea is to tune the major and minor axes of the ellipse for x- and y-polarizations to achieve independent phase controllability at dual bands while maintaining high transmission characteristics. The preliminary results of this work are presented in [33]. This present paper is organized as follows. The characterization of the proposed unitcell in terms of transmission parameters is presented in Section 2. The simulated and measured results of the dual-band MTS lens are presented in Section 3. Finally, the conclusions are outlined in Section 4.

2. UNITCELL DESIGN AND ANALYSIS

The unit cell consists of an elliptical patch encircled by a square ring printed on an FR4 substrate ($\epsilon_r = 4.4$) as shown in Figure 1. Each unit cell consists of four identical metallization layers on three-layer dielectric surfaces sandwiched together to enhance the transmission phase coverage of MTS [17, 34]. The unitcell analysis is carried out in CST Microwave Studio with unit cell boundary conditions along x- and y-directions. Two orthogonal Floquet modes are used to excite the unitcell.

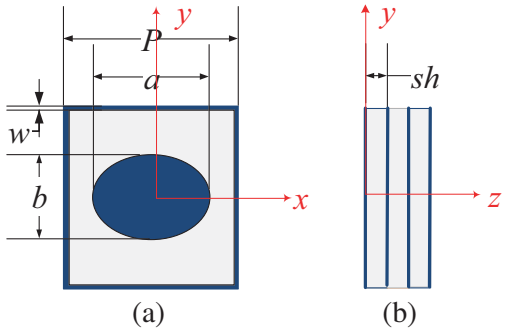

Figure 1. Unitcell dimensions (mm) are given as $P = 9$, $w = 0.2$, $sh = 0.8$. (a) Top view. (b) Side view.

The simulated transmission response of the unit cell ($a = 6$, $b = 6.5$) as a function of frequency is shown in Figure 2(a). It is evident from the figure that $|S_{21}|$ is greater than 0.8 in the frequency range of 8–10 GHz for x-polarized incident wave with a phase variation from $-100°$ to $-450°$. It can also be seen that $|S_{21}|$ drops significantly beyond 10.1 GHz for x-polarized incident wave, hence, the unitcell behaves like a reflector beyond 10.1 GHz. Similar behavior has been observed for y-polarized incident wave in the frequency range of 10–12 GHz. The co-polarized reflection coefficient is minimum in both the cases till 10.1 GHz and 12.2 GHz for x- and y-polarizations, respectively. Hence, only co-polarized transmission coefficients are considered in the design process. Figure 2(b) shows the variation of transmission response as a function of angle of incidence. It can be seen that the unitcell offers stable

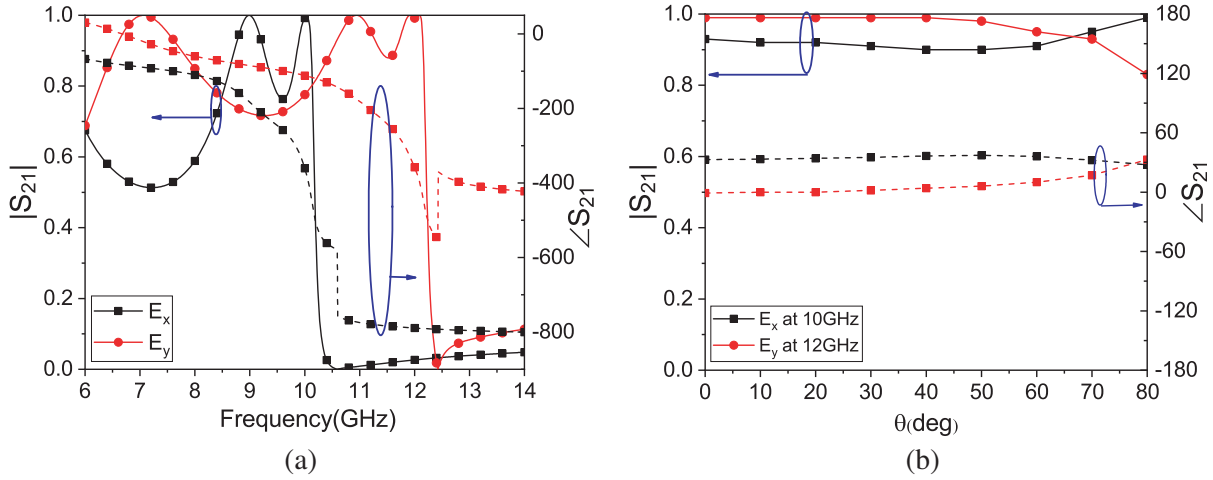

Figure 2. Simulation results: transmission response. (a) Variation of frequency. (b) Variation of incidence angle ($a = 8\,\text{mm}$, $b = 6.5\,\text{mm}$).

transmission characteristics for different angles of incidence (θ) at the desired frequency of operation, i.e., 10 and 12 GHz.

It is desired to achieve a 360° phase variation at the design frequency for proper operation of the PGMS lens. In order to cover a full 360° phase variation, the design parameters a is varied from 4 to 8 mm and b varied from 2 to 6.5 mm with an interval of 0.02 mm with fixed periodicity ($P = 9\,\text{mm}$) of the unitcell. Figure 3(a) shows the transmission characteristics by keeping $b = 6.5\,\text{mm}$ and varying a at 10 GHz for x-polarization and 12 GHz for y-polarization. It can be seen that for x-polarization, $|S_{21}| \geq 0.65$ with phase varying from $-40°$ to $-380°$. Hence, the unitcell offers a stable amplitude response with a phase span of 340° for x-polarized incident wave at 10 GHz. The effects of a variation for y-polarization are minimal at 12 GHz, and a stable amplitude response is observed with maximum phase deviation of 60°. Figure 3(b) shows a similar behavior by varying b and keeping $a = 8\,\text{mm}$ for y-polarization at 12 GHz. Again, a 380° phase coverage is realized with a high transmission coefficient. It is observed that the transmission response gets affected with increasing angle of incidence for all the (a, b). However, the transmission coefficient remains relatively constant for the angle of incidence less than 60°. A database of the transmission characteristics for all the variations of unitcell parameters is created to realize the required phase for PGMS design.

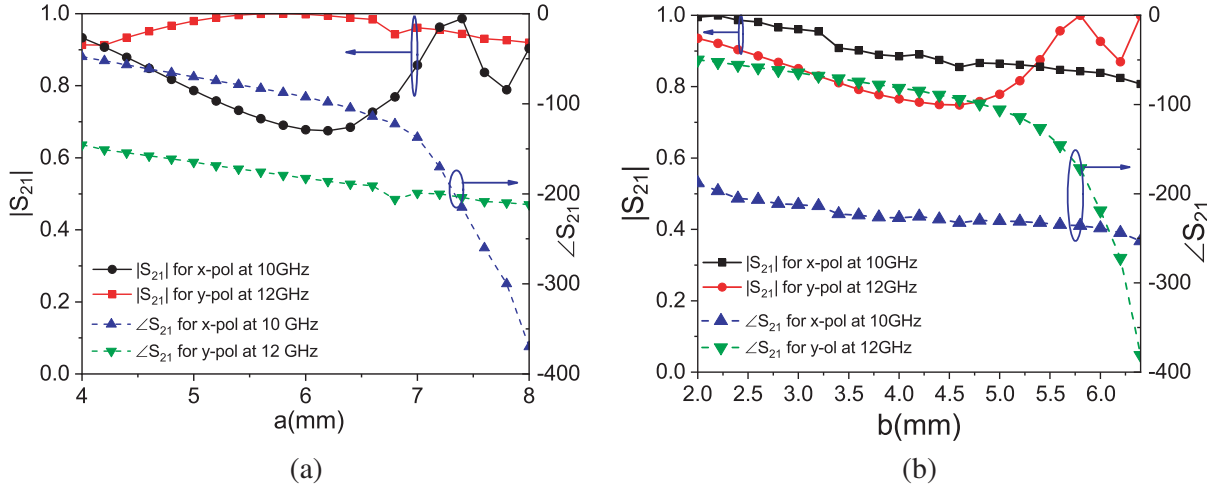

Figure 3. Simulation results. (a) Variation of a at 10 GHz with $b = 6.5\,\text{mm}$. (b) Variation of b at 12 GHz with $a = 8\,\text{mm}$.

3. ANISOTROPIC PGMS DESIGN FOR GAIN ENHANCEMENT

The gain enhancement is achieved by collimating the beam in broadside direction using the phase compensation method. Figure 4(a) shows the arrangement of the MTS and the antenna. At a given frequency and focal distance, the phase on the PGMS is given by [34],

$$\psi_{mn} = k(R_{mn} - \overrightarrow{r}_{mn} \cdot \hat{u}) + \psi_0 \tag{1}$$

where ψ_{mn} is the phase at the (m,n)th position, k the free space wave number, R_{mn} the distance between the feed position and the (m,n)th element, $\overrightarrow{r}_{mn}$ the position vector of (m,n)th element, and θ_e the angle of incidence. The parameter ψ_0 is the phase at the MTS center. Hence, ψ_{mn} indicates the relative phase rather than the absolute phase on the MTS [34]. In this analysis, an MTS of 15×15 unitcells with $\psi_0 = 0°$ is considered. The phase on the MTS is a function of feed location (F) and beam direction $\hat{u}$. The phase profiles required for 10 GHz and 12 GHz for a given focal point are calculated based on Eq. (1). The required phase profile is matched with the unitcell database for x- and y-polarized incident waves.

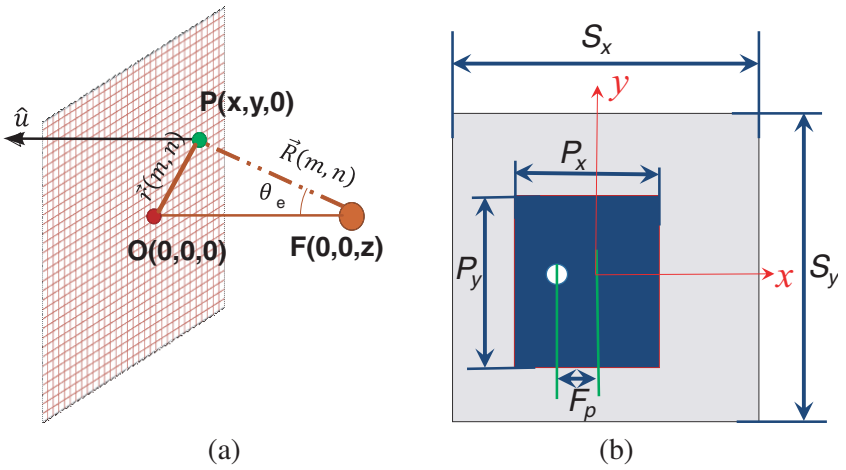

Figure 4. Gain enhancement using phase compensation method. (a) MTS and antenna alignment. (b) Geometry of the feed (patch antenna).

For the analysis of the MTS, a dual-band antenna with a broadside radiation pattern having orthogonal polarization purity needs to be placed at the focal point for simultaneous gain enhancement in two frequency bands. A dual-band patch antenna with orthogonal polarization may be designed to demonstrate the performance of the MTS lens. However, the primary concern of the current study is to realize dual-band high gain MTS, and for simplicity, we have demonstrated the performance of MTS by two independent patch antennas operating at two operating frequencies. Hence, two linearly polarized patch antennas operating at 10 GHz and 12 GHz are considered and labeled as antenna-1 and antenna-2, respectively. Antenna-1 and antenna-2 are placed at focal point (F) with radiating edge aligned along x- and y-directions, respectively. The patch antenna is printed on an FR4 substrate having a thickness of 1.6 mm with $\tan\delta = 0.004$ and shown in Figure 4(b). The design parameters of antenna-1 and antenna-2 are reported in Table 1.

Table 1. Dimensions of the patch antennas (all the dimensions are in mm).

Antenna	Frequency	S_x	S_y	P_x	P_y	F_p
Antenna-1	10 GHz	15	15	6.25	7	1.6
Antenna-2	12 GHz	15	15	6	6	1.4

Figures 5(a) and 5(b) show the calculated phase distributions at 10 GHz and 12 GHz, respectively. The MTS is designed with one-to-one phase mapping of a and b from the database at 10 GHz and 12 GHz, respectively. Figure 6 shows the designed and fabricated MTSs. As the patch antenna is not an ideal point source and MTS not a 2D sheet, the focal point is not exactly located at 30 mm from the center of MTS. As the theoretical analysis suggests that the gain is maximum at the focal distance, the feed position is varied from 30 mm to 40 mm with an interval of 2 mm. An optimal distance of 35 mm is found for the maximum gain, hence, 35 mm focal distance is in all the simulations. Therefore, the ratio of focal distance to the dimension (F/D) is 0.19.

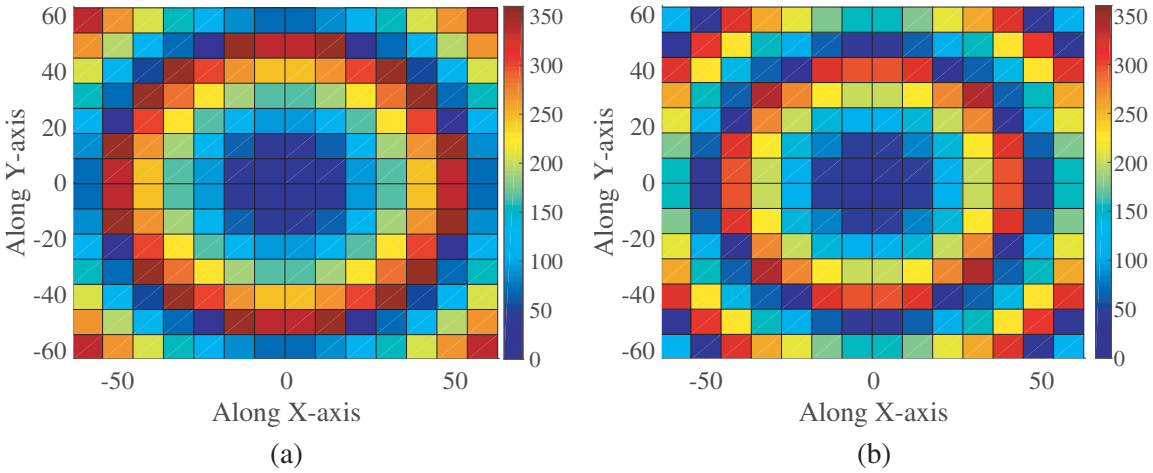

Figure 5. MTS design: Phase profile (a) at 10 GHz, (b) at 12 GHz.

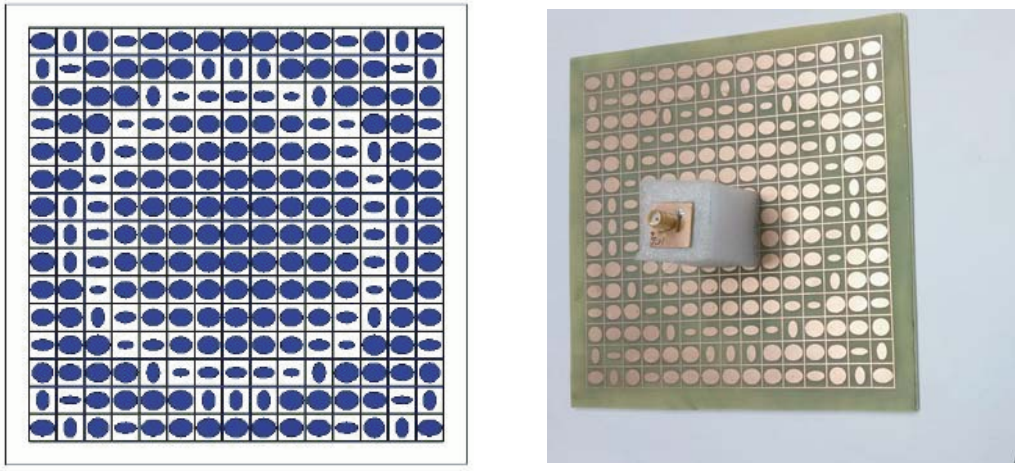

Figure 6. MTS lens antenna. (a) Designed PGMS. (b) Fabricated PGMS lens antenna.

Reflection coefficients for the two different antennas with MTS are shown in Figure 7(a). The black and blue curves represent the simulated and measured responses of antenna-1 with MTS for x-polarized incident wave. Similarly, red and green curves show the simulated and measured results of antenna-2 with MTS for y-polarized incident wave. It is observed that the antenna reflection coefficient is less than -15 dB at both the operating frequencies. A slight shift in the S_{11} response is observed between the simulated and measured results due to the fabrication tolerance of antenna and MTS.

Figure 7(b) shows the simulated and measured gains of the antenna with and without MTS. In the figure, solid lines are used to represent the simulated results, and dashed lines are used to represent the

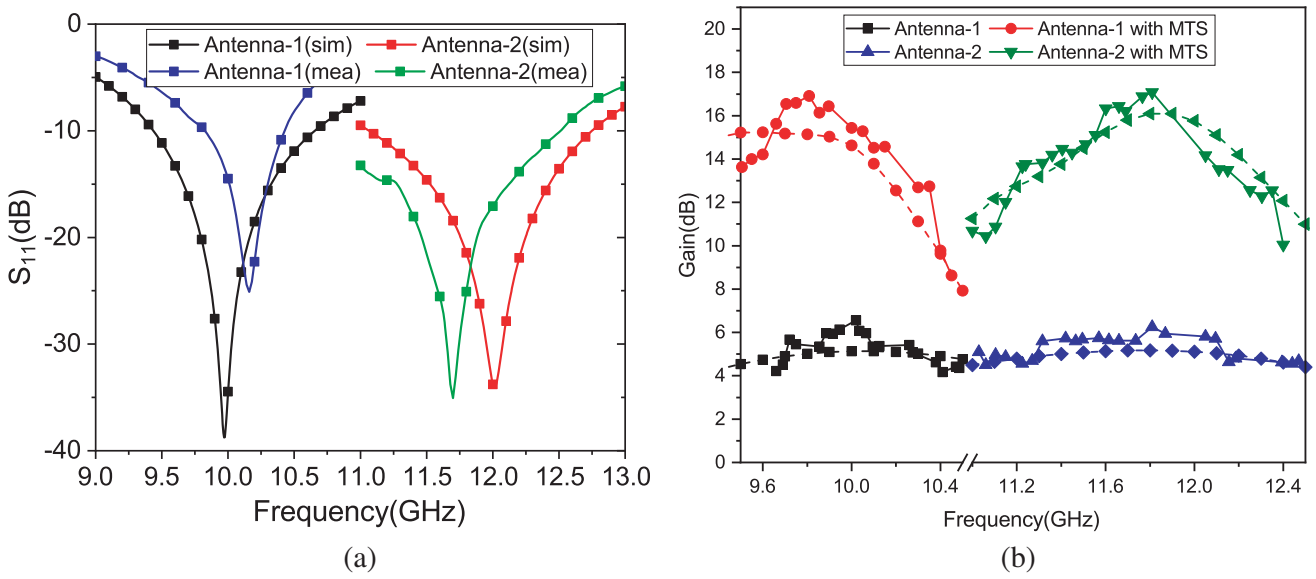

Figure 7. Simulated and measured results with and without MTS. (a) Reflection coefficient. (b) Gain variation with respect to frequency (Simulation and measured results are represented in solid and dash lines, respectively).

measured results. The black and blue lines represent the gains of patch antennas without the MTS. The gains of antenna-1 and antenna-2 with MTS are depicted by red and green curves, respectively. It is evident from the figure that an average gain enhancement of 10 dB is observed in the frequency range of [9.5–10.1] GHz and [11.6–12.1] GHz, respectively. Although the MTS and antennas are designed at 10 and 12 GHz, it is found that the maximum gain is obtained at 9.8 GHz and 11.8 GHz. Hence, the radiation characteristics of the MTS antenna are presented for these frequencies. The measured peak gain of the PGMS lens antennas is around 11.5 dB relative to the feed at 9.8 GHz and 11.8 GHz. The simulated and measured radiation patterns at 9.8 GHz and 11.8 GHz in $\phi = 0$ and $\phi = 90^\circ$ plane are

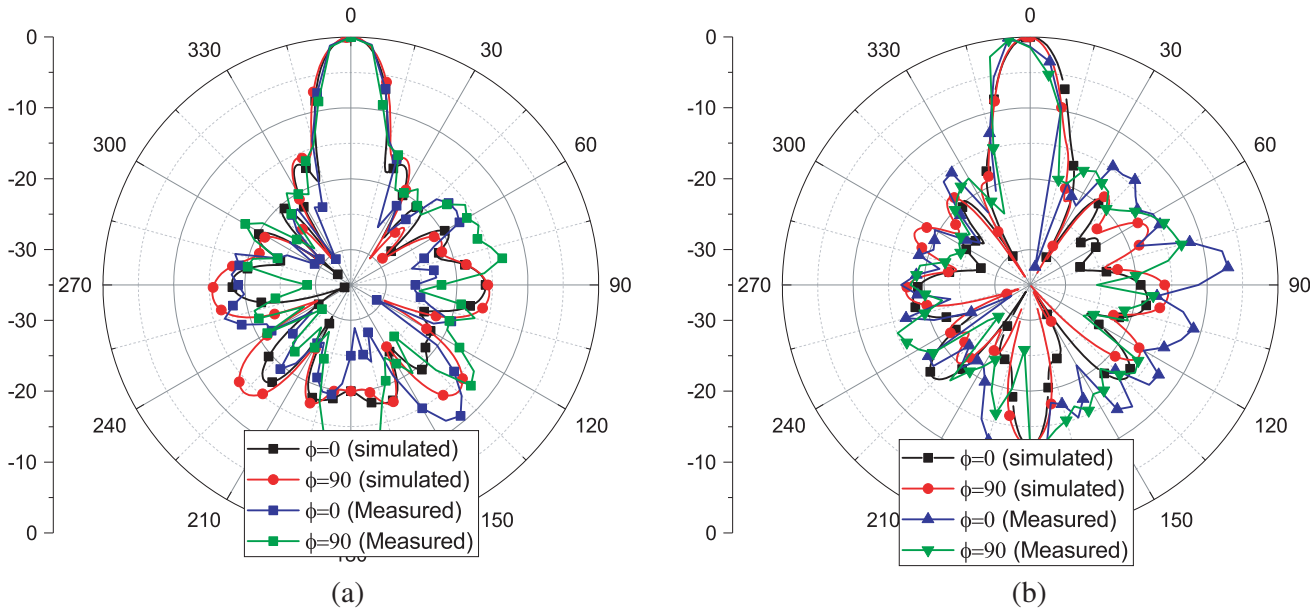

Figure 8. Simulated and measured radiation pattern (a) at 9.8 GHz, (b) 11.8 GHz.

shown in Figure 8. At 9.8 GHz, the simulated side-lobe-level (SLL) is −16 dB in both $\phi = 0°$ and $\phi = 90°$ planes with a front to back ratio −25 dB, whereas the measured SLL is given by −18 dB and −19 dB in $\phi = 0°$ and $\phi = 90°$ planes, respectively. At 11.8 GHz, simulated SLL is given by −19 dB in $\phi = 0°$ plane and −18 dB in $\phi = 90°$ plane with front to back ratio of −15 dB, as compared to the measured SLL of −16 and −18 dB SLL in $\phi = 0°$ and $\phi = 90°$ planes, respectively. The simulated efficiency of the antenna is found to be nearly 60% at both the operating frequencies. The typical radiation characteristics of the antenna with MTS are reported in Table 2. A comparison of the present work with the earlier works on multi-band lens antennas is tabulated in Table 3.

Table 2. Gain enhancement of the MTS.

Property	x-polarization	y-polarization
Frequency (GHz)	9.8	11.8
Directivity (dB)	17.7	20.1
θ_{peak} (deg)	0	0
SLL (dB)	18	20.1
Beam width (deg)	13.2	11.4
Efficiency(%)	60	61

Table 3. Performance comparison table with other multi-band lens antennas.

	[22]	[30]	[31]	[32]	Proposed structure
MTS Type	R (CP)	T/T	T/T	T/T	T/T
Center frequency (GHz)	7.1/8.4/32	12.5/17.5	10/14	6.5/10.5	10/12
Gain Enhancement (dB)	13.4/14.1/23	10/8	8.8/8.2	13.1/9.2	11.5/11.5
F/D ratio	0.9	1	0.25	0.25	0.19
SLL (dB)	-/-/-	12/11.9	-/-	15.3/15.3	18/18
Unitcell number		169	221	169	225
Dimension (λ is the lowest frequency)	$13.4\lambda \times 13.4\lambda$	$9.2\lambda \times 9.2\lambda$	$6.2\lambda \times 7.3\lambda$	$2.8\lambda \times 2.8\lambda$	$4.5\lambda \times 4.5\lambda$

T = Transmission type MTS; R = Reflection type MTS; F/D = ratio of focal length (F) to the dimension (D); LP/CP = Linear/Circular Polarization

4. CONCLUSION

A dual-band high gain MTS lens antenna has been designed and analyzed in the X-band. The MTS consists of 15 × 15 unitcells occupying 135 × 135 mm^2 having a focal point at 30 mm from the center of the MTS. The high transmittance and compensated phase profile give an average gain enhancement of 10 dB for all MTSs in two different frequency regions. The bandwidth of the system is limited by the properties of narrow band antenna and unitcells. The proposed antenna offers dual-band gain enhancement with polarization purity, lower SLL, and low F/D ratio. The performance of the PGMS remains same irrespective of feeding antenna; however, the polarization of the incident wave and the feed position need to be taken care for achieving the gain enhancement with low SLL. Thus, this work can efficiently fit into the development of multi-functional antennas using polarization dependent MTS. The beam direction can also be changed simultaneously with the present approach by recalculating the phase profile on the MTS.

REFERENCES

1. Chahat, N., E. Decrossas, D. Gonzalez-Ovejero, O. Yurduseven, M. J. Radway, R. E. Hodges, P. Estabrook, J. D. Baker, D. J. Bell, T. A. Cwik, et al., "Advanced cubesat antennas for deep space and earth science missions: A review," *IEEE Antennas and Propagation Magazine*, Vol. 61, No. 5, 37–46, 2019.
2. Hodges, R. E., N. Chahat, D. J. Hoppe, and J. D. Vacchione, "A deployable high-gain antenna bound for Mars: Developing a new folded-panel reflectarray for the first CubeSat mission to Mars," *IEEE Antennas and Propagation Magazine*, Vol. 59, No. 2, 39–49, 2017.
3. Babuscia, A., T. Choi, J. Sauder, A. Chandra, and J. Thangavelautham, "Inflatable antenna for CubeSats: Development of the X-band prototype," *2016 IEEE Aerospace Conference*, 1–11, IEEE, 2016.
4. Hodges, R. E., D. J. Hoppe, M. J. Radway, and N. E. Chahat, "Novel deployable reflectarray antennas for CubeSat communications," *2015 IEEE MTT-S International Microwave Symposium*, 1–4, IEEE, 2015.
5. Sauder, J. F., M. Arya, N. Chahat, E. Thiel, S. Dunphy, M. Shi, G. Agnes, and T. Cwik, "Deployment mechanisms for high packing efficiency One-Meter Reflectarray Antenna (OMERA)," AIAA Scitech 2019 Forum, 0755, 2019.
6. Minatti, G., F. Caminita, E. Martini, M. Sabbadini, and S. Maci, "Synthesis of modulated-metasurface antennas with amplitude, phase, and polarization control," *IEEE Transactions on Antennas and Propagation*, Vol. 64, No. 9, 3907–3919, 2016.
7. Patel, A. M. and A. Grbic, "Modeling and analysis of printed-circuit tensor impedance surfaces," *IEEE Transactions on Antennas and Propagation*, Vol. 61, No. 1, 211–220, 2012.
8. Szabo, Z., G.-H. Park, R. Hedge, and E.-P. Li, "A unique extraction of metamaterial parameters based on Kramers-Kronig relationship," *IEEE Transactions on Microwave Theory and Techniques*, Vol. 58, No. 10, 2646–2653, 2010.
9. Cai, T., G.-M. Wang, X.-F. Zhang, J.-G. Liang, Y.-Q. Zhuang, D. Liu, and H.-X. Xu, "Ultra-thin polarization beam splitter using 2-D transmissive phase gradient metasurface," *IEEE Transactions on Antennas and Propagation*, Vol. 63, No. 12, 5629–5636, 2015.
10. Lee, Y., S.-J. Kim, H. Park, and B. Lee, "Metamaterials and metasurfaces for sensor applications," *Sensors*, Vol. 17, No. 8, 1726, 2017.
11. Joy, V., A. Dileep, P. Abhilash, R. U. Nair, and H. Singh, "Metasurfaces for stealth applications: A comprehensive review," *Journal of Electronic Materials*, 1–20, 2021.
12. Afzal, M. U. and K. P. Esselle, "Steering the beam of medium-to-high gain antennas using near-field phase transformation," *IEEE Transactions on Antennas and Propagation*, Vol. 65, No. 4, 1680–1690, 2017.
13. Ding, F., A. Pors, and S. I. Bozhevolnyi, "Gradient metasurfaces: A review of fundamentals and applications," *Reports on Progress in Physics*, Vol. 81, No. 2, 026401, 2017.
14. Erfani, E., M. Niroo-Jazi, and S. Tatu, "A high-gain broadband gradient refractive index metasurface lens antenna," *IEEE Transactions on Antennas and Propagation*, Vol. 64, No. 5, 1968–1973, 2016.
15. Junyao, W., F. Junpeng, S. Hao, L. Chang, and C. Yongzhi, "Efficiency-tunable terahertz focusing lens based on graphene metasurface," *Opto-Electronic Engineering*, Vol. 48, No. 04, 200319, 2021.
16. He, B., J. Fan, Y. Cheng, F. Chen, H. Luo, and R. Gong, "Thermally tunable terahertz vortex beam generator based on an InSb metasurface," *JOSA B*, Vol. 38, No. 5, 1518–1524, 2021.
17. Li, H., G. Wang, H.-X. Xu, T. Cai, and J. Liang, "X-band phase-gradient metasurface for high-gain lens antenna application," *IEEE Transactions on Antennas and Propagation*, Vol. 63, No. 11, 5144–5149, 2015.
18. Pang, Y., Y. Li, B. Qu, M. Yan, J. Wang, S. Qu, and Z. Xu, "Wideband RCS reduction metasurface with a transmission window," *IEEE Transactions on Antennas and Propagation*, Vol. 68, No. 10, 7079–7087, 2020.

19. Chen, H.-T., A. J. Taylor, and N. Yu, "A review of metasurfaces: physics and applications," *Reports on Progress in Physics*, Vol. 79, No. 7, 076401, 2016.
20. Liang, J.-J., G.-L. Huang, J.-N. Zhao, Z.-J. Gao, and T. Yuan, "Wideband phase-gradient metasurface antenna with focused beams," *IEEE Access*, Vol. 7, 20 767–20 772, 2019.
21. Pfeiffer, C. and A. Grbic, "Cascaded metasurfaces for complete phase and polarization control," *Applied Physics Letters*, Vol. 102, No. 23, 231116, 2013.
22. Nayeri, P., F. Yang, and A. Z. Elsherbeni, *Reflectarray Antennas: Theory, Designs, and Applications*, 2018.
23. Yang, F., Y. Kim, J. Huang, and A. Elsherbeni, "A single-layer tri-band reflectarray antenna design," *2007 IEEE Antennas and Propagation Society International Symposium*, 5307–5310, IEEE, 2007.
24. Ren, Y., Y. Lu, T. Zang, Y. Wang, Y. Dai, and P. Wang, "Multi-mode resonance properties of two-dimensional metal-dielectric-metal fishnet metasurface at visible wavelengths," *Optics Express*, Vol. 25, No. 23, 28 417–28 426, 2017.
25. Ghaderi, B., V. Nayyeri, M. Soleimani, and O. M. Ramahi, "Pixelated metasurface for dual-band and multi-polarization electromagnetic energy harvesting," *Scientific Reports*, Vol. 8, No. 1, 1–12, 2018.
26. Ma, H. F., G. Z. Wang, G. S. Kong, and T. J. Cui, "Independent controls of differently-polarized reflcted waves by anisotropic metasurfaces," *Scientific Reports*, Vol. 5, 9605, 2015.
27. Jia, S. L., X. Wan, D. Bao, Y. J. Zhao, and T. J. Cui, "Independent controls of orthogonally polarized transmitted waves using a Huygens metasurface," *Laser & Photonics Reviews*, Vol. 9, No. 5, 545–553, 2015.
28. Fan, J. and Y. Cheng, "Broadband high-efficiency cross-polarization conversion and multi-functional wavefront manipulation based on chiral structure metasurface for terahertz wave," *Journal of Physics D: Applied Physics*, Vol. 53, No. 2, 025109, 2019.
29. Fan, J., Y. Cheng, and B. He, "High-efficiency ultrathin terahertz geometric metasurface for full-space wavefront manipulation at two frequencies," *Journal of Physics D: Applied Physics*, Vol. 54, No. 11, 115101, 2021.
30. Zainud-Deen, S., S. Gaber, H. Malhat, and K. Awadalla, "Single feed dual-polarization dual-band transmitarray for satellite applications," *2013 30th National Radio Science Conference (NRSC)*, 27–34, IEEE, 2013.
31. Li, H.-P., G.-M. Wang, X.-J. Gao, J.-G. Liang, and H.-S. Hou, "An X/Ku-band focusing anisotropic metasurface for low cross-polarization lens antenna application," *Progress In Electromagnetics Research*, Vol. 159, 79–91, 2017.
32. Cai, T., G.-M. Wang, J.-G. Liang, Y.-Q. Zhuang, and T.-J. Li, "High-performance transmissive meta-surface for C-/X-band lens antenna application," *IEEE Transactions on Antennas and Propagation*, Vol. 65, No. 7, 3598–3606, 2017.
33. Kumar, P. V. and B. Ghosh, "A dual-band multi-layer metasurface lens,"*2018 IEEE Indian Conference on Antennas and Propogation (InCAP)*, 1–4, IEEE, 2018.
34. Abdelrahman, A. H., F. Yang, A. Z. Elsherbeni, and P. Nayeri, "Analysis and design of transmitarray antennas," *Synthesis Lectures on Antennas*, Vol. 6, No. 1, 1–175, 2017.